Interfacial engineering to improve Cu_2ZnSnX_4 (X = S, Se) solar cell efficiency

Cite as: APL Mater. 7, 091104 (2019); doi: 10.1063/1.5116623
Submitted: 26 June 2019 • Accepted: 15 August 2019 •
Published Online: 6 September 2019

H. J. Gu,[1,2] J.-H. Yang,[1] S. Y. Chen,[3] H. J. Xiang,[1,2] and X. G. Gong[1,2]

AFFILIATIONS

[1]Key Laboratory for Computational Physical Sciences (MOE), State Key Laboratory of Surface Physics, Department of Physics, Fudan University, Shanghai 200433, China
[2]Collaborative Innovation Center of Advanced Microstructures, Nanjing 210093, China
[3]Key Laboratory of Polar Materials and Devices (MOE), East China Normal University, Shanghai 200241, China

ABSTRACT

Interfacial properties between metal back contacts and solar cell absorbers play important roles in determining efficiencies, but studies of such properties in CZTS and CZTSe based solar cells are quite lacking from theoretical aspects. To fill such a blank and explore insights for improving energy conversion efficiencies, we have studied interfacial properties in CZTS and CZTSe solar cells. The natural band offsets between CZTX and the spontaneously formed MoX_2 layer (X = S, Se) are obtained using our recently developed intermediate-phase method. We find that the band alignment between CZTS and MoS_2 is actually harmful while the band alignment between CZTSe and $MoSe_2$ is beneficial for carrier extractions. We further propose to engineer the back contact interface to improve CZTS solar cell efficiency by depositing a thin layer of Se on the Mo back contact prior to the CZTS deposition, thus avoiding the formation of the undesirable MoS_2 layer.

INTRODUCTION

Quaternary compounds such as CZTS and CZTSe in the kesterite structure have attracted intensive interest during the past decades as they have shown great promise for low-cost solar cell absorbers.[1–8] They exhibit high absorption coefficients and suitable direct bandgaps, and the constituent elements are naturally abundant and nontoxic.[1–5] According to Shockley-Queisser theory, they have very high energy conversion efficiencies, i.e., the theoretical maximum efficiencies of CZTSe and CZTS solar cells are 31% and 32.4%,[9] respectively. However, their practical efficiencies are quite unsatisfactory. So far, CZTSe solar cells have reached a record efficiency of 11.6%,[10] while efficiencies of CZTS solar cells were long stagnant at around 9%[11,12] and reached 11%[13] only until recently. Solar cells based on CZTSSe alloys have achieved an energy conversion efficiency of 12.6%,[4] which is the highest efficiency in this family. Apparently, such experimental efficiencies are quite far below their theoretical maximum values, leaving much room for improvement.

To understand the efficiency-limiting factors of CZTSSe based solar cells, various comparable studies of CZTS and CZTSe have been made both experimentally and theoretically in order to get helpful insights, from many perspectives including the defect levels, the bandgap size, and the doping ability of the isolated bulk materials, with several effective performance-optimizing strategies proposed.[14,15] While the above studies mainly focused on properties of isolated solar cell absorber materials, it is known that interfacial properties between solar cell absorbers and back contacts also play critical roles in determining solar cell efficiencies. However, as far as we know, such studies in CZTX solar cells are quite limited, especially from the theoretical aspect.

The conventional back contact used for CZTS is the Mo layer, borrowed from the more mature CIGS solar cells.[16] Many experiments have proved that Mo is a unique back contact material for CIGS solar cells.[17–19] Besides its low electrical resistivity, the interfacial layer $MoSe_2$ formed spontaneously between Mo back contact and CIGS absorber was observed experimentally to facilitate the formation of an ohmic transport system between CIGS and Mo back contact, thus helping to reduce the series resistance of CIGS solar cells.[17,18] Many studies claimed that the beneficial $MoSe_2$ interlayer in the CIGS solar cell system accounts for one important reason for its high conversion efficiency.[18,19] Similarly, it has been observed

that an interfacial layer MoS_2 ($MoSe_2$) forms spontaneously during the CZTS (CZTSe) absorber layer deposition on top of the Mo back contact.[10,20,21] However, the exact effect of the MoS_2 ($MoSe_2$) layer on the performance of the CZTS (CZTSe) solar cells, e.g., how they affecting the carrier extraction process, is still unclear.

In order to understand the impact of the MoS_2 ($MoSe_2$) interfacial layer on the CZTS (CZTSe) based solar cells and obtain more insights into enhance the efficiencies, one key point is to obtain the natural band offsets between CZTX and MoX_2 (X = S, Se), which is of great importance for understanding the carrier transport properties in the heterojunctions. Previously, the natural band offset between two systems was usually computed by constructing a heterostructure superlattice to avoid the energy reference problem in infinite systems, and this method works very well for systems with similar symmetry.[14,22–25] However, because CZTX and MoX_2 (X = S, Se) have totally different lattices, it is almost impossible to construct their heterostructure superlattice, making the determination of their natural band offsets unsettled so far. In this paper, we address this problem by adopting the intermediate-phase method for the band offset calculation. We create an intermediate phase which matches with both CZTS and MoS_2 (similarly for the CZTSe/$MoSe_2$ system). In the rest of the paper, we first introduce the methods for computing the natural band offset and then present the calculated results and discussions of the band alignments between CZTS (CZTSe) and MoS_2 ($MoSe_2$).

INTERMEDIATE-PHASE METHOD

The intermediate-phase method is a general method to calculate the band offset between any two semiconductors. Based on the core-level alignment calculation,[22,23] the valence band offset between two hypothetical structures L and R is given by

$$\Delta E_v(L/R) = \Delta E^R_{v,C^*} - \Delta E^L_{v,C} + \Delta E^{L/R}_{C,C^*}, \quad (1)$$

where $\Delta E^R_{v,C^*}$ and $\Delta E^L_{v,C}$ are energy differences between the core levels of R and L to their valence band maximum (VBM), respectively, which can be obtained by bulk calculations. $\Delta E^{L/R}_{C,C^*}$ is the core level difference between L and R calculated using a L/R superlattice. This method works very well for systems with a negligible lattice mismatch.[14,24,25] However, for systems with a larger lattice mismatch, the volume deformation influence on $\Delta E^{L/R}_{C,C^*}$ has to be considered by taking the absolute deformation potential (APD) corrections into account,[26–28] which is difficult to obtain and is only practical for some special lattices. In order to get band offsets of systems with a larger lattice mismatch, Lang *et al.* recently proposed the three-step method.[29] In this method, the core-level alignment $\Delta E^{L/R}_{C,C^*}$ for two structures L and R with lattice constants (a_1, a_2, a_3) and (b_1, b_2, b_3), respectively, is obtained using the following three steps. In the first step, L is stretched (or compressed) along the [100] direction to L' with lattice constants (b_1, a_2, a_3). Then, $\Delta E^{L/L'}_{C,C'}$ can be calculated using an L/L' superlattice along the [100] direction. Similarly, in the second step, L' *is* stretched (or compressed) along the [010] direction to L'' with lattice constants (b_1, b_2, a_3) so that $\Delta E^{L'/L''}_{C',C''}$ can be obtained. In the last step, $\Delta E^{L''/R}_{C'',C^*}$ can be calculated using an L''/R superlattice. The above procedures make sure that every superlattice in every step has no lattice-mismatch problem. Finally, the valence band offset between L and R is given by

$$\Delta E_v(L/R) = \Delta E^R_{v,C^*} - \Delta E^L_{v,C} + \Delta E^{L/L'}_{C,C'} + \Delta E^{L'/L''}_{C',C''} + \Delta E^{L''/R}_{C'',C^*}. \quad (2)$$

While the three-step method avoids the difficulty of direct calculations of absolute deformation potentials, it is, in general, limited to systems with similar structures for which superlattices are easily formed. However, for systems with totally different structures, such as diamond and graphite, it is nearly impossible to construct a heterostructure. In this case, computing band offset values using the above superlattice methods becomes invalid. To solve this problem, we recently proposed a new method called the intermediate-phase method.[30] For any two semiconductors L and R, we can create an intermediate phase C with one surface that matches L and another surface that matches R, and then we use the three-step method to calculate the band offsets between L and C and between R and C. Finally, the band offset between L and R is obtained by

$$\Delta E_v(L/R) = \Delta E_v(L/C) + \Delta E_v(C/R). \quad (3)$$

Note that the intermediate phase between L and R is not unique. According to the transitivity rule,[31] all the different intermediate phases should give approximately the same value for $\Delta E_v(L/R)$, subject to the condition that all the interfaces are well built. In many cases, when the structures of L and R are not simple, finding a proper intermediate phase is a significant challenge. We have previously proposed an algorithm based on differential evolution to search for intermediate phases according to the target properties of a good intermediate phase: low binding energy, large bandgap (so that the electrons are localized and have smaller tendency to transfer across the interface, and thus the interfacial effect on the core level alignment calculation can be reduced), and good structural and constituent match with the two end-point structures (i.e., L and R).[30] Combining the intermediate-phase method with the three-step method, in principle, one can calculate the band offset between any two semiconductors.

CALCULATION DETAILS

In this work, the structural relaxation and electronic structure calculations are performed based on the density functional theory (DFT) method. The ion-electron interaction is treated by the projector augmented-wave (PAW) technique,[32] as implemented in the Vienna *ab initio* simulation package (VASP).[33] The exchange-correlation potential is treated with the Perdew-Burke-Ernzerhof (PBE) functional.[34] The plane-wave basis set cutoff is 500 eV. The k-mesh is generated by the Monkhorst-Pack scheme,[35] and the spacing of k-points is approximately $0.03 \times 2\pi$ Å^{-1}

For the CZTS and MoS_2 system, we noticed that the CZTS (001) surface has the same symmetry as the (001) surface of a zinc-blende structure, meanwhile the (001) surface of MoS_2 is hexagonally close-packed and has the same symmetry as the (111) surface of a zinc-blende structure. Consequently, we constructed the compound C_1 of copper-zinc-tin-sulfur in the zinc-blend structure as the intermediate phase to match both CZTS and MoS_2 after adjusting the lattice constants following the three-step method. In addition, we found C_1 has a bandgap of 1.41 eV calculated by PBE functional, well satisfying the requirement for a good intermediate phase to

TABLE I. Lattice parameters (Å) and space groups of CZTS (CZTSe), MoS_2 ($MoSe_2$), and the intermediate phase C_1 (C_2). The lattice parameters of CZTS (CZTSe) and MoS_2 ($MoSe_2$) are fully optimized by the PBE calculations.

Name	a	b	c	α	β	γ	Space group
CZTS	5.47	5.47	10.94	90	90	90	$I\bar{4}$ [82]
MoS_2	3.18	3.18	14.38	90	90	120	$P6_3/mmc$ [194]
C_1	4.50	4.50	4.50	90	90	90	$P\bar{4}2m$ [111]
CZTSe	5.77	5.77	11.53	90	90	90	$I\bar{4}$ [82]
$MoSe_2$	3.32	3.32	15.06	90	90	120	$P6_3/mmc$ [194]
C_2	4.70	4.70	4.70	90	90	90	$P\bar{4}2m$ [111]

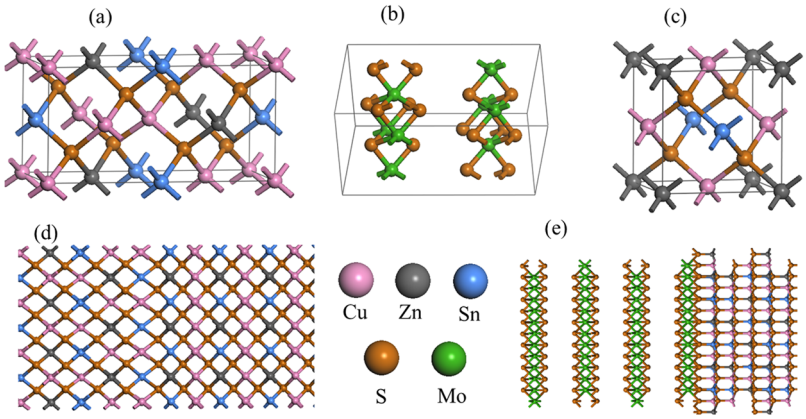

FIG. 1. Bulk structures of (a) CZTS, (b) MoS_2, and (c) the intermediate phase C_1 (Cu_2ZnSnS_4), and heterostructures of (d) CZTS″(001)/C_1(001) and (e) MoS_2(001)/C_1(111). CZTS″ is deformed from CZTS in the three-step method to make its (001) surface match with C_1(001). Pink, gray, blue, brown, and green spheres represent Cu, Zn, Sn, S, and Mo atoms, respectively.

have a larger bandgap as possible. Similarly, the copper-zinc-tin-selenium compound in the zinc-blend structure C_2, with a PBE bandgap of 0.94 eV, has been taken as the intermediate phase for the CZTSe/$MoSe_2$ system. The lattice parameters of the intermediate phases C_1 and C_2 are listed in Table I. The structures of the crystals and interfaces are shown in Fig. 1. The computational procedure is schematically shown in Fig. 2(a).

RESULTS AND DISCUSSION

Our calculated result shows that the valence band edge of CZTS is 0.33 eV higher than that of MoS_2. Considering that the experimental bandgaps are 1.50 eV[36,37] and 1.29 eV[38] for CZTS and MoS_2, respectively, we can conclude that the conduction band minimum (CBM) of CZTS is 0.54 eV higher than that of MoS_2, as illustrated in Fig. 2(b). This type-II band alignment means that holes from the VBM of CZTS have to overcome a barrier of 0.33 eV in order to transfer across the MoS_2 interlayer toward the Mo back contact, meanwhile electrons tend to accumulate in the CBM of MoS_2, leading to the enhancement of recombination with the holes from the anode material CZTS. On the other hand, for the CZTSe/$MoSe_2$ system with experimental bandgaps of 1.00 eV[39] and 1.10 eV,[40,41] respectively, our calculated result also suggests a type-II band offset but with the VBM and CBM of CZTSe both lower than those of $MoSe_2$ by 0.13 eV and 0.23 eV, respectively, as illustrated in Fig. 2(c). Such a band alignment naturally helps the charge separation with holes transferring to $MoSe_2$ and electrons transferring to CZTSe, which is beneficial for the CZTSe solar cell efficiency.

To further verify our results, we calculated the band offsets of CZTS/CZTSe and MoS_2/$MoSe_2$ using the three-step method and obtained the valence band offsets of −0.07 eV and −0.45 eV, respectively. According to the transitivity rule, we have that

$$\begin{aligned}\Delta E_v^{three-step}(\mathrm{MoSe_2}-\mathrm{MoS_2})+\Delta E_v^{three-step}(\mathrm{CZTS}-\mathrm{CZTSe})\\ =\Delta E_v^{three-step}(\mathrm{MoSe_2}-\mathrm{CZTSe})+\Delta E_v^{three-step}(\mathrm{CZTS}-\mathrm{MoS_2})\\ =0.38\ \mathrm{eV}.\end{aligned}$$

Based on the valence band offsets of the CZTS/MoS_2 and CZTSe/$MoSe_2$ systems obtained by the intermediate-phase method, we get that

$$\begin{aligned}\Delta E_v^{intermediate-phase}(\mathrm{MoSe_2}-\mathrm{CZTSe})+\Delta E_v^{intermediate-phase}\\ (\mathrm{CZTS}-\mathrm{MoS_2})=0.46\ \mathrm{eV},\end{aligned}$$

generally in line with the results of the three-step method calculation.

To understand why the VBM of CZTS is above that of MoS_2 while for CZTSe/$MoSe_2$, it is the opposite, we look into the electronic properties of the four materials. We find that the VBMs of CZTS, MoS_2, CZTSe, and $MoSe_2$ are all antibonding states and are dominated by Cu 3d and S 3p, Mo 4d and S 3p, Cu 3d and Se 4p, and Mo 4d and Se 4p, respectively (see Fig. 3). Generally speaking, there are two factors accounting for the positions of antibonding states. One is the original atomic levels. If all the other conditions are the same, higher atomic levels always tend to form higher bonding and antibonding states. The other factor is the strength of the

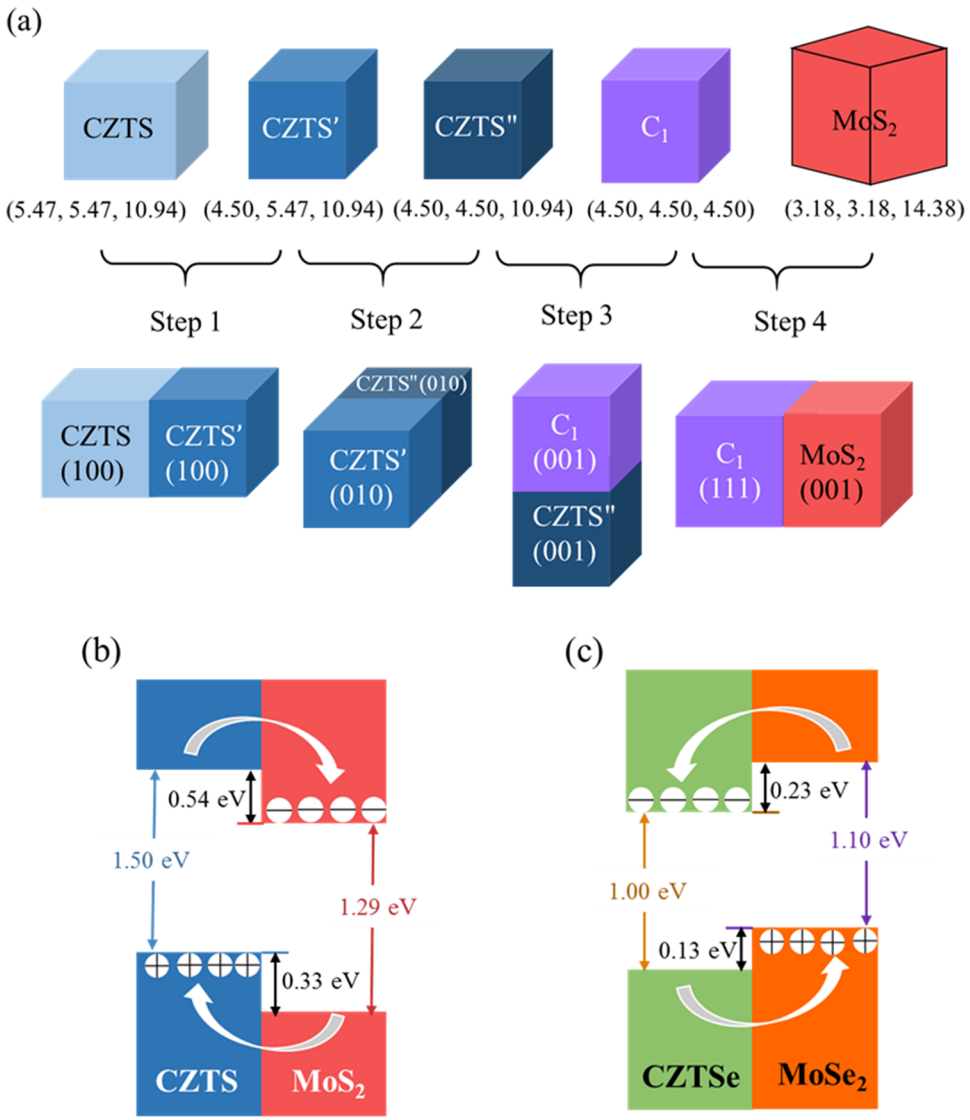

FIG. 2. (a) The procedures for calculating the valence band offset between CZTS and MoS_2 using the intermediate phase C_1. In the first two steps, the lattice of CZTS is compressed to match with C_1. In the last two steps, the heterostructures of CZTS″/C_1 and MoS_2/C_1 are constructed. Lattice constants (Å) are listed below the sketch models of crystals. (b) and (c) The valence and conduction band alignments of CZTS/MoS_2 and CZTSe/$MoSe_2$ systems, respectively. The arrows indicate the transfer of electrons and holes in the conduction and valence bands, respectively.

interaction (or overlap) between the atomic orbitals. Stronger interactions between atomic orbitals can lower the bonding states while raising the antibonding states. Generally, the strength of the interaction is related to the energy difference between atomic energy levels, that is, closer atomic levels can lead to stronger interactions. The atomic levels of Cu 3d, S 3p, Se 4p, and Mo 4d are listed in Fig. 3(e).[42] Based on these atomic energy levels, we can qualitatively illustrate the different valence band edge alignments of CZTS/MoS_2 and CZTSe/$MoSe_2$ heterostructures by considering the above two factors. For the CZTS/MoS_2 system, the energy level of Mo 4d is much higher than Cu 3d, but the energy level of Cu 3d is nearly equal to S 3p. Therefore, the interaction between Cu and S atoms is strong enough to raise the VBM of CZTS higher than that of MoS_2. For the CZTSe/$MoSe_2$ system, the energy difference between Cu 3d and Se 4p is larger than that between Cu 3d and S 3p, indicating a weaker interaction between Cu and Se atoms than that between Cu and S atoms. Similarly, the energy difference between Se 4p and Mo 4d is smaller than that between S 3p and Mo 4d, suggesting that the interaction between Se and Mo atoms is stronger than that between S and Mo atoms. Consequently, the interaction between Se and Cu atoms is not strong enough to raise the VBM of CZTSe higher than that of $MoSe_2$.

Our calculated results have shown that the band alignment between the CZTSe absorber and the $MoSe_2$ layer is beneficial for charge transfer to the Mo back contact, while the band alignment of CZTS/MoS_2 is harmful. This could also be a reason why CZTS solar cells are less efficient than CZTSe solar cells experimentally although the theoretical maximum efficiency of CZTS solar cells is higher. Dhakal *et al.*[16] also measured the band alignment between Mo, MoS_2, and CZTS experimentally and proved that MoS_2 could be a barrier to hole-transport at the MoS_2/CZTS interface, which agrees with our calculated result. Some experiments have also found

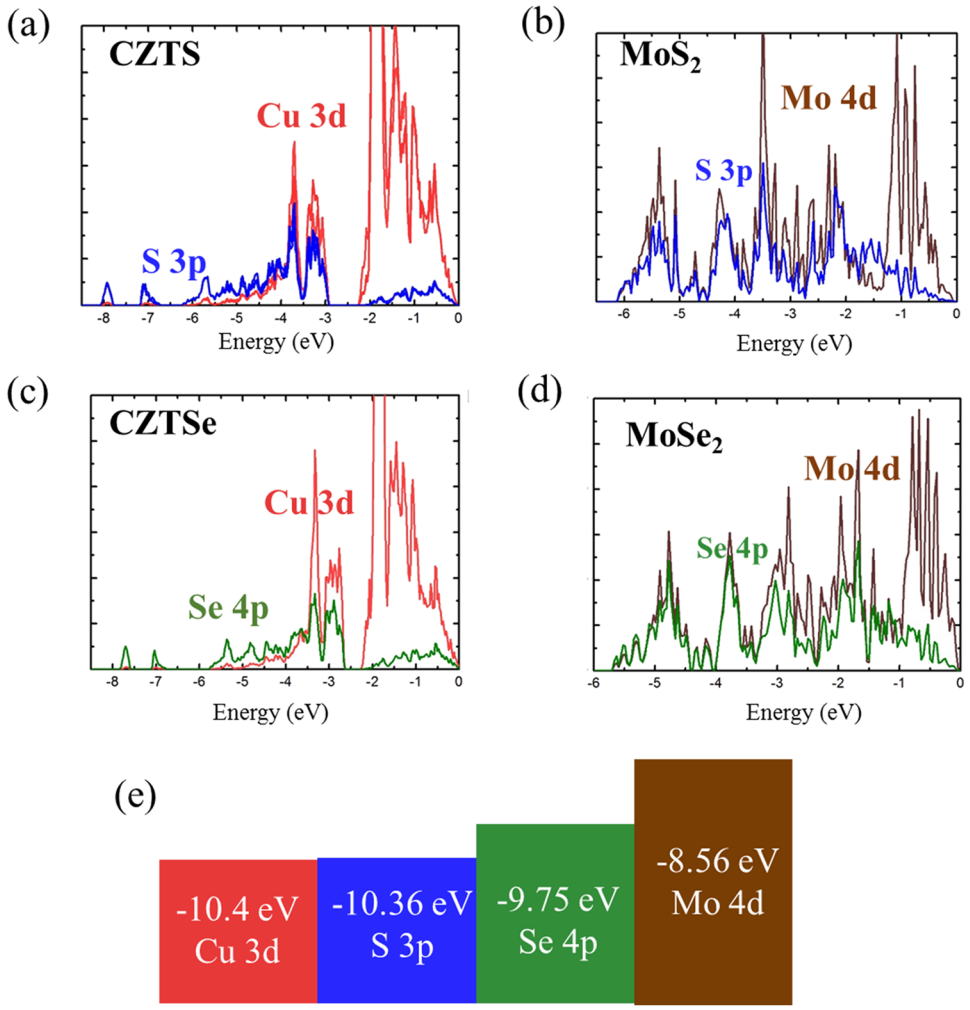

FIG. 3. Calculated electronic density of states of (a) CZTS, (b) MoS_2, (c) CZTSe, and (d) $MoSe_2$, respectively, with the VBM set to be 0 eV. (e) The atomic energy levels of Cu 3d, S 3p, Se 4p, and Mo 4d.

that the thick MoS_2 interlayer is responsible for high series resistance in the CZTS device.[43,44] Consequently, the MoS_2 layer at the back contact should be reduced to improve solar cell efficiencies. We also notice that several experiments have tried to control the formation of the MoS_2 layer by deposition of a barrier between CZTS and Mo to avoid S diffusion through the Mo. For example, Cui *et al.* used the Ag layer as the barrier,[44] which, despite showing encouraging improvement of the device performance, is not suitable for a large-scale production. TiN has also been used as the barrier layer;[45] however, it introduces extra resistance at the CZTS/TiN interface. The highest efficiency (11%) reported so far for the pure CZTS solar cell is obtained by using an ultrathin Al_2O_3 layer as a barrier to reduce MoS_2 thickness.[13] Here, based on our above study, we propose to deposit a thin layer of Se on the Mo back contact prior to CZTS deposition for the following reasons. (i) The predeposited Se layer on Mo back contact will form a layer of $MoSe_2$, thus inhibiting S diffusion to Mo back contact. (ii) The preformed $MoSe_2$ layer could benefit holes transferring to the Mo back contact. (iii) $MoSe_2$ and MoS_2 have the same symmetry and very close lattice constants, and the interfacial structure between the CZTS absorber and the Mo back contact is not expected to change much and introduce disadvantageous effects on solar cell performance using the predeposition of Se so that the beneficial effects can be largely expected. By modifying the interface at the back contact, one can expect to improve the efficiency of CZTS solar cells to a higher level.

CONCLUSION

In conclusion, we have provided theoretical studies of interfacial properties between Mo back contact and CZTX solar cell absorbers. We have comparably studied the effect of Mo back contact on CZTS and CZTSe solar cells by calculating the natural band offset between CZTX and MoX_2 (X = S, Se) using the intermediate-phase method. We find that both systems show a type-II band alignment, with the VBM of CZTS 0.33 eV higher than that of MoS_2 and the VBM of CZTSe 0.13 eV lower than that of $MoSe_2$. Our results indicate that the MoS_2 interlayer formed between the CZTS absorbers can block holes from transferring to the Mo back contact; thus, it is harmful for the performance of CZTS solar cells. On the contrary, the $MoSe_2$ interlayer is beneficial for the CZTSe solar cell.

We propose to deposit a thin layer of Se on the Mo back contact prior to the CZTS deposition to avoid the disadvantageous impact of the MoS_2 layer. Our work provides some deeper understanding of CZTX (X = S, Se) solar cells and will be useful for the further improvement of CZTX (X = S, Se) solar cell efficiencies.

ACKNOWLEDGMENTS

This work was supported by the Special Funds for Major State Basic Research (Nos. 2016YFB0700701 and 2016YFA0301001), the National Natural Science Foundation of China (NSFC), the Program for Professor of Special Appointment (Eastern Scholar), and the Qing Nian Ba Jian Program. J.-H. Yang was sponsored by the Fudan Start-up funding (Grant No. JIH1512034) and the Shanghai Sailing Program (Grant No. 19YF1403100).

REFERENCES

[1] X. Liu, Y. Feng, H. Cui, F. Liu, X. Hao, G. Conibeer, D. B. Mitzi, and M. Green, Prog. Photovoltaics **24**(6), 879–898 (2016).
[2] A. Redinger, D. M. Berg, P. J. Dale, R. Djemour, L. Guetay, T. Eisenbarth, N. Valle, and S. Siebentritt, IEEE J. Photovoltaics **1**(2), 200–206 (2011).
[3] A. Haddout, A. Raidou, and M. Fahoume, Appl. Phys. A **125**(2), 124 (2019).
[4] W. Wang, M. T. Winkler, O. Gunawan, T. Gokmen, T. K. Todorov, Y. Zhu, and D. B. Mitzi, Adv. Energy Mater. **4**(7), 1301465 (2014).
[5] K. Kaur, N. Kumar, and M. Kumar, J. Mater. Chem. A **5**(7), 3069–3090 (2017).
[6] S. Hartnauer, S. Koerbel, M. A. L. Marques, S. Botti, P. Pistor, and R. Scheer, APL Mater. **4**(7), 070701 (2016).
[7] J. M. Skelton, A. J. Jackson, M. Dimitrievska, S. K. Wallace, and A. Walsh, APL Mater. **3**(4), 041102 (2015).
[8] J. Just, D. Luetzenkirchen-Hecht, O. Mueller, R. Frahm, and T. Unold, APL Mater. **5**(12), 126106 (2017).
[9] W. Ki and H. W. Hillhouse, Adv. Energy Mater. **1**(5), 732–735 (2011).
[10] Y. S. Lee, T. Gershon, O. Gunawan, T. K. Todorov, T. Gokmen, Y. Virgus, and S. Guha, Adv. Energy Mater. **5**(7), 1401372 (2015).
[11] B. Shin, O. Gunawan, Y. Zhu, N. A. Bojarczuk, S. J. Chey, and S. Guha, Prog. Photovoltaics **21**(1), 72–76 (2013).
[12] S. Tajima, M. Umehara, M. Hasegawa, T. Mise, and T. Itoh, Prog. Photovoltaics **25**(1), 14–22 (2017).
[13] C. Yan, J. Huang, K. Sun, S. Johnston, Y. Zhang, H. Sun, A. Pu, M. He, F. Liu, K. Eder, L. Yang, J. M. Cairney, N. J. Ekins-Daukes, Z. Hameiri, J. A. Stride, S. Chen, M. A. Green, and X. Hao, Nat. Energy **3**(9), 764–772 (2018).
[14] S. Chen, A. Walsh, J.-H. Yang, X. G. Gong, L. Sun, P.-X. Yang, J.-H. Chu, and S.-H. Wei, Phys. Rev. B **83**(12), 125201 (2011).
[15] S. Chen, A. Walsh, X.-G. Gong, and S.-H. Wei, Adv. Mater. **25**(11), 1522–1539 (2013).
[16] T. P. Dhakal, S. Harvey, M. van Hest, G. Teeter, and IEEE, in *2015 IEEE 42nd Photovoltaic Specialist Conference* (IEEE, 2015).
[17] L. Assmann, J. C. Bernede, A. Drici, C. Amory, E. Halgand, and M. Morsli, Appl. Surf. Sci. **246**(1-3), 159–166 (2005).
[18] T. Wada, N. Kohara, S. Nishiwaki, and T. Negami, Thin Solid Films **387**(1-2), 118–122 (2001).
[19] D. Abou-Ras, G. Kostorz, D. Bremaud, M. Kalin, F. V. Kurdesau, A. N. Tiwari, and M. Dobeli, Thin Solid Films **480**, 433–438 (2005).
[20] J. T. Watjen, J. J. Scragg, T. Ericson, M. Edoff, and C. Platzer-Bjorkman, Thin Solid Films **535**, 31–34 (2013).
[21] B. Shin, N. A. Bojarczuk, and S. Guha, Appl. Phys. Lett. **102**(9), 091907 (2013).
[22] S. H. Wei and A. Zunger, Appl. Phys. Lett. **72**(16), 2011–2013 (1998).
[23] S. H. Wei and A. Zunger, Phys. Rev. Lett. **59**(1), 144–147 (1987).
[24] S. Chen, X. G. Gong, and S.-H. Wei, Phys. Rev. B **75**(20), 205209 (2007).
[25] Q. Shu, J.-H. Yang, S. Chen, B. Huang, H. Xiang, X.-G. Gong, and S.-H. Wei, Phys. Rev. B **87**(11), 115208 (2013).
[26] Y.-H. Li, A. Walsh, S. Chen, W.-J. Yin, J.-H. Yang, J. Li, J. L. F. Da Silva, X. G. Gong, and S.-H. Wei, Appl. Phys. Lett. **94**(21), 212109 (2009).
[27] Y.-H. Li, X. G. Gong, and S.-H. Wei, Phys. Rev. B **73**(24), 245407 (2006).
[28] Y. H. Li, X. G. Gong, and S. H. Wei, Appl. Phys. Lett. **88**(4), 042104 (2006).
[29] L. Lang, Y.-Y. Zhang, P. Xu, S. Chen, H. J. Xiang, and X. G. Gong, Phys. Rev. B **92**(7), 075102 (2015).
[30] H. J. Gu, Y. Y. Zhang, S. Y. Chen, H. J. Xiang, and X. G. Gong, Phys. Rev. B **97**(23), 235308 (2018).
[31] C. G. Van De Walle and R. M. Martin, Phys. Rev. B **35**(15), 8154–8165 (1987).
[32] P. E. Blochl, Phys. Rev. B **50**(24), 17953–17979 (1994).
[33] G. Kresse and J. Furthmuller, Comput. Mater. Sci. **6**(1), 15–50 (1996).
[34] J. P. Perdew, K. Burke, and M. Ernzerhof, Phys. Rev. Lett. **77**(18), 3865–3868 (1996).
[35] H. J. Monkhorst and J. D. Pack, Phys. Rev. B **13**(12), 5188–5192 (1976).
[36] B.-A. Schubert, B. Marsen, S. Cinque, T. Unold, R. Klenk, S. Schorr, and H.-W. Schock, Prog. Photovoltaics **19**(1), 93–96 (2011).
[37] K. Tanaka, N. Moritake, and H. Uchiki, Sol. Energy Mater. Sol. Cells **91**(13), 1199–1201 (2007).
[38] K. F. Mak, C. Lee, J. Hone, J. Shan, and T. F. Heinz, Phys. Rev. Lett. **105**(13), 136805 (2010).
[39] D. Park, D. Nam, S. Jung, S. An, J. Gwak, K. Yoon, J. H. Yun, and H. Cheong, Thin Solid Films **519**(21), 7386–7389 (2011).
[40] J. C. Shaw, H. Zhou, Y. Chen, N. O. Weiss, Y. Liu, Y. Huang, and X. Duan, Nano Res. **7**(4), 511–517 (2014).
[41] H. Ahmad, M. A. Ismail, S. Sathiyan, S. A. Reduan, N. E. Ruslan, C. S. Lee, M. Z. Zulkifli, K. Thambiratnam, M. F. Ismail, and S. W. Harun, Opt. Commun. **382**, 93–98 (2017).
[42] T. A. Carlson, *Photoelectron and Auger Spectroscopy* (Plenum, New York, 1975).
[43] W. Li, J. Chen, H. Cui, F. Liu, and X. Hao, Mater. Lett. **130**, 87–90 (2014).
[44] H. Cui, X. Liu, F. Liu, X. Hao, N. Song, and C. Yan, Appl. Phys. Lett. **104**(4), 041115 (2014).
[45] J. J. Scragg, T. Kubart, J. T. Watjen, T. Ericson, M. K. Linnarsson, and C. Platzer-Bjorkman, Chem. Mater. **25**(15), 3162–3171 (2013).